The Astrophysical Journal Letters, 885:L26 (6pp), 2019 November 1 https://doi.org/10.3847/2041-8213/ab4b5a

Mechanism of Reconnection on Kinetic Scales Based on *Magnetospheric Multiscale* Mission Observations

W. M. Macek[1,2,3], M. V. D. Silveira[1,4], D. G. Sibeck[1], B. L. Giles[1], and J. L. Burch[5]
[1] NASA Goddard Space Flight Center, Code 6740, Greenbelt, MD 20771, USA
[2] Faculty of Mathematics and Natural Sciences, Cardinal Stefan Wyszyński University, Wóycickiego 1/3, 01-938 Warsaw, Poland; macek@uksw.edu.pl
[3] Space Research Centre, Polish Academy of Sciences, Bartycka 18 A, 00-716 Warsaw, Poland; macek@cbk.waw.pl
[4] Catholic University of America, Washington, DC 20064, USA; marcosvinicius.diassilveira@nasa.gov
[5] Southwest Research Institute, San Antonio, TX, USA; jburch@swri.edu
Received 2019 May 6; revised 2019 October 7; accepted 2019 October 7; published 2019 November 1

Abstract

We examine the role that ions and electrons play in reconnection using observations from the *Magnetospheric Multiscale* (*MMS*) mission on kinetic ion and electron scales, which are much shorter than magnetohydrodynamic scales. This study reports observations with unprecedented high resolution that *MMS* provides for magnetic field (7.8 ms) and plasma (30 ms for electrons and 150 ms for ions). We analyze and compare approaches to the magnetopause in 2016 November, to the electron diffusion region in the magnetotail in 2017 July followed by a current sheet crossing in 2018 July. Besides magnetic field reversals, changes in the direction of the flow velocity, and ion and electron heating, *MMS* observed large fluctuations in the electron flow speeds in the magnetotail. As expected from numerical simulations, we have verified that when the field lines and plasma become decoupled a large reconnecting electric field related to the Hall current (1–10 mV m^{-1}) is responsible for fast reconnection in the ion diffusion region. Although inertial accelerating forces remain moderate (1–2 mV m^{-1}), the electric fields resulting from the divergence of the full electron pressure tensor provide the main contribution to the generalized Ohm's law at the neutral sheet (as large as 200 mV m^{-1}). In our view, this illustrates that when ions decouple electron physics dominates. The results obtained on kinetic scales may be useful for better understanding the physical mechanisms governing reconnection processes in various magnetized laboratory and space plasmas.

Key words: Earth – magnetic fields – magnetic reconnection – methods: data analysis – plasmas

Turbulent magnetic fields play an important role in plasmas, e.g., leading to magnetic reconnection (Vasyliunas 1975; Burlaga 1995; Biskamp 2000; Treumann 2009; Figura & Macek 2013; Treumann & Baumjohann 2013), and the redistribution of kinetic and magnetic energy in space environments and laboratory plasmas. Reconnection occurs when the electrons cannot supply the current needed to support antiparallel magnetic fields. This is a complex phenomenon that still remains a challenge for contemporary physics. Notwithstanding great progress in magnetohydrodynamic (MHD; Hall–MHD, two-fluid) simulations, the physical mechanisms for reconnection are still not clearly understood. The dynamic variability of plasma and fields at very small electron scales in the solar system is not well known. However, collisionless space and astrophysical plasmas can be considered natural laboratories for investigating the complex dynamics (Bruno & Carbone 2016). Moreover, reconnection processes may play an important role in mixing heliospheric and interstellar plasmas, as postulated by Macek & Grzedzielski (1985), a hypothesis supported by numerical simulations (Strumik et al. 2013, 2014). Reconnection at the heliopause, which is the ultimate boundary separating the heliosphere from the very local interstellar medium, has yet to be confirmed by experimental data.

One of the main objectives of the *Magnetospheric Multiscale* (*MMS*) mission is to determine the role of turbulence in the reconnection processes and the roles of ions and electrons in these processes. The *MMS* mission may also be useful for better understanding the physical mechanisms governing reconnection processes in various laboratory and space plasmas. Evidence for the reconnection diffusion region on the dayside magnetopause using *MMS* measurements has recently been found by Burch et al. (2016b) in a case study on 2016 October 16, which was further discussed by Torbert et al. (2016). Kinetic simulations of magnetopause reconnection have also been reported by Daughton et al. (2014), while simulation results for a magnetotail case are provided by Nakamura et al. (2018). *MMS* observations of an electron-scale magnetic cavity embedded in a proton-scale cavity have been recently reported (Liu et al. 2019). One can hence expect that a detailed analysis of the high-resolution *MMS* data can provide better insight into the nature of reconnection processes in space plasmas.

Magnetopause reconnection is relatively easy to recognize. A list of 32 such magnetopause events has been reported by Webster et al. (2018). Observations of electron-scale structures and magnetic reconnection signatures in the turbulent magnetosheath using *MMS* measurements have been provided by Yordanova et al. (2016), and reconnection jets at the magnetopause have been analyzed by Øieroset et al. (2016). Because the tail is highly dynamic and nightside reconnection is limited to the vicinity of the current sheet, it is much more difficult to find reconnection events here. A current sheet on electron scales in the near-Earth magnetotail without bursty reconnection has been identified by Wang et al. (2018). The first tail reconnection event on 2017 July 11 was reported by Torbert et al. (2018). Although *MMS* barely resolves electron scales during reconnection, the latter authors reported that the spacecraft entered the electron diffusion region (EDR) in the magnetotail, suggesting that the electron dynamics in

this region was mostly laminar despite turbulence near the reconnection region. Even if the spacecraft remains in the much larger ion diffusion region (IDR), one can can study reconnection from approaches to the EDR in the tail current sheet.

Therefore, this Letter focuses on the deviations from MHD, including Hall–MHD, electron pressure, and inertia effects on both ion and electron scales as seen in the *MMS* data. Following our previous study of turbulence and reconnection using *MMS* data (Macek et al. 2018, 2019), we analyze in greater detail the electric fields on sub-ion scales at the magnetopause and in the magnetotail near the *X*-line within highly variable plasmas to compare the characteristics of reconnection processes in both regions when going from the ion to electron kinetic scales. This naturally leads to a description of space plasmas within kinetic theory, instead of an ideal MHD approach.

We find experimental evidence for a somewhat turbulent (chaotic) reconnection in the magnetotail, as suggested by numerical simulations (see, e.g., Lazarian et al. 2015 and references therein). We observe rather large reconnecting electric fields resulting from the Hall currents for the plasma and magnetic field data at the highest resolution available within the *MMS* mission (see Yamada et al. 2016). The additional components are caused by a moderate inertial term followed by large pressure forces activated when approaching the reconnection site. Basically, the electric field related to the full electron pressure tensor becomes the main contribution there, showing that when ions decouple electron kinetic physics dominates.

In the classical one-fluid MHD theory the electric field $\boldsymbol{E}_{\rm o}{}' = \boldsymbol{E} + \boldsymbol{V} \times \boldsymbol{B} = \boldsymbol{R}$, seen in the rest frame by the plasma moving with the velocity $\boldsymbol{V}$, is often described by the ideal case ($\boldsymbol{R} = 0$; see, e.g., Krall & Trivelpiece 1973). In two-fluid theory, the sum of all the contributions to the electric field, $\boldsymbol{E}_{\rm tot}$, consisting of various terms should be equal to the dissipation created by an anomalous resistivity η in the generalized Ohm's law. Basically, one should have (see Rossi & Olbert 1970, Equation (12.25))

$$\boldsymbol{E}_{\rm tot} = \boldsymbol{E}'_{\rm o} + \boldsymbol{E}_{\rm H} + \boldsymbol{E}_{\rm a} + \boldsymbol{E}_{\rm p} = \eta \boldsymbol{j}, \tag{1}$$

where $\boldsymbol{E}_{\rm H}$, $\boldsymbol{E}_{\rm a}$, and $\boldsymbol{E}_{\rm p}$ denote the Hall, inertial, and pressure terms. Namely, the electric fields responsible for dissipative processes at reconnection sites must be described by nonideal terms (e.g., Baumjohann & Treumann 1996; Biskamp 2000; Yamada et al. 2016). Using the quasi-neutrality of plasma with density $n = n_{\rm i} = n_{\rm e}$ (and the electron to ion mass ratio $m_{\rm e}/m_{\rm i} \ll 1$), the bulk velocity of the plasma is approximately equal to the velocity of ions, $\boldsymbol{V} \approx \boldsymbol{V}_{\rm i}$, provided that the velocities of ions and electrons are of the same order of magnitude, $\boldsymbol{V}_{\rm i} \sim \boldsymbol{V}_{\rm e}$.

For many astrophysical applications inside the ion IDR the main contribution to the electric field should come from the Hall term, $\boldsymbol{E}_{\rm H} = -\boldsymbol{j} \times \boldsymbol{B}/(en)$, with the current density $\boldsymbol{j} = e(n_{\rm i}\boldsymbol{V}_{\rm i} - n_{\rm e}\boldsymbol{V}_{\rm e})$ (e is the electron elementary charge). Since $\boldsymbol{E}_{\rm H} = (\boldsymbol{V}_{\rm e} - \boldsymbol{V}_{\rm i}) \times \boldsymbol{B}$ taking $\boldsymbol{V} \approx \boldsymbol{V}_{\rm i}$ we have

$$\boldsymbol{E}' \equiv \boldsymbol{E}'_{\rm o} + \boldsymbol{E}_{\rm H} = \boldsymbol{E} + \boldsymbol{V} \times \boldsymbol{B} + \boldsymbol{E}_{\rm H} \approx \boldsymbol{E} + \boldsymbol{V}_{\rm e} \times \boldsymbol{B}. \tag{2}$$

This means that electrons remain frozen and are convected by the magnetic field. It is worth noting that the Hall term is active on kinetic ion scales (Burch et al. 2016a). On the other hand, the new $\boldsymbol{E}_{\rm a}$ and $\boldsymbol{E}_{\rm p}$ terms describing the electric field resulting from the difference between accelerated electrons and ions and the thermal pressure of electrons relative to the ion background, respectively, should be important on both ion and electron scales (Spitzer 1956; Rossi & Olbert 1970). Therefore, these two other inertia and thermal terms should also be important in the kinetic regime.

In the reconnection region, the inertial forces resulting from separation of the electrons and ions should be taken into account. The first nonideal component to the electric field should come from the difference of the acceleration of electrons and ions $e\boldsymbol{E}_{\rm a} = m_{\rm e} d(\boldsymbol{V}_{\rm e} - \boldsymbol{V}_{\rm i})/dt$. Namely, taking the time and space change of the convective derivative of the electrons $\left(\frac{d}{dt} \equiv \frac{\partial}{\partial t} + \boldsymbol{V}_{\rm e} \cdot \boldsymbol{\nabla}\right)$ and ion $\left(\frac{d}{dt} \equiv \frac{\partial}{\partial t} + \boldsymbol{V}_{\rm i} \cdot \boldsymbol{\nabla}\right)$ for jets moving rapidly from the *X*-line for both the electron $\boldsymbol{V}_{\rm e}$ and ion $\boldsymbol{V}_{\rm i}$ flows, turning electrons and ions from inflowing into outflowing current directions, we have $(e/m_{\rm e})\boldsymbol{E}_{\rm a} = \left[\left(\frac{\partial}{\partial t} + \boldsymbol{V}_{\rm e} \cdot \boldsymbol{\nabla}\right)\boldsymbol{V}_{\rm e} - \left(\frac{\partial}{\partial t} + \boldsymbol{V}_{\rm i} \cdot \boldsymbol{\nabla}\right)\boldsymbol{V}_{\rm i}\right]$. Next, using the continuity conservation equations, $\frac{\partial n}{\partial t} + \boldsymbol{\nabla} \cdot (n\boldsymbol{V}) = 0$, for both the ion and electron fluxes, one obtains the following formula for steady-state conditions:

$$\boldsymbol{E}_{\rm a} = \frac{m_{\rm e}}{\rm e}\left\{\frac{1}{n_{\rm e}}\boldsymbol{\nabla} \cdot [n_{\rm e}(\boldsymbol{V}_{\rm e} \cdot \boldsymbol{V}_{\rm e})] - \frac{1}{n_{\rm i}}\boldsymbol{\nabla} \cdot [n_{\rm i}(\boldsymbol{V}_{\rm i} \cdot \boldsymbol{V}_{\rm i})]\right\}, \tag{3}$$

corresponding to the conservation of the total anisotropic kinetic energy density flux in the stress tensor, which involves the divergence $\boldsymbol{\nabla}$ of this tensor (Landau et al. 1984).

The second (nonideal) contribution to the electric field results from the divergence of the fully anisotropic pressure (dyadic) tensor (e.g., Gurnett & Bhattacharjee 2005, Equation (5.1.7)), $\boldsymbol{P} \equiv m\int (\boldsymbol{V} - \boldsymbol{U})(\boldsymbol{V} - \boldsymbol{U}) f d^3\boldsymbol{V}$. Note that by averaging over velocity space for a given position $\boldsymbol{r} = (x, y, z)$ within an infinitesimally small fluid element of volume $d^3\boldsymbol{r} = dxdydz$, one can write $\boldsymbol{P} = mn\langle(\boldsymbol{V} - \boldsymbol{U})(\boldsymbol{V} - \boldsymbol{U})\rangle$ (see Spitzer 1956, Equation (2.6)). This means that the pressure term should have a somewhat similar structure to that of the inertial term, as given by Equation (3), but with the distribution function f for individual particles moving randomly with velocities $\boldsymbol{V}$ around the mean (bulk) velocity $\boldsymbol{U} \equiv \langle \boldsymbol{V} \rangle = \frac{1}{n}\int \boldsymbol{V} f d^3\boldsymbol{V}$. Because $m_{\rm e}/m_{\rm i} \ll 1$, the contribution from the ion pressure tensor can be neglected and we only have the electron tensor electric field (e.g., Rossi & Olbert 1970):

$$\boldsymbol{E}_{\rm p} \equiv \frac{1}{{\rm e}n_{\rm e}}\boldsymbol{\nabla} \cdot \boldsymbol{P}_{\rm e} = \frac{m_{\rm e}}{{\rm e}n_{\rm e}}\boldsymbol{\nabla} \cdot [n_{\rm e}\langle(\boldsymbol{V}_{\rm e} - \boldsymbol{U})(\boldsymbol{V}_{\rm e} - \boldsymbol{U})\rangle], \tag{4}$$

where the diagonal thermal pressures are given by $p_{\parallel {\rm e}} = n_{\rm e} k T_{\parallel {\rm e}}$ and $p_{\perp {\rm e}} = n_{\rm e} k T_{\perp {\rm e}}$, parallel and perpendicular with regard to the magnetic field $\boldsymbol{B}$, and k is the Boltzmann constant, $T_{\parallel {\rm e}} + 2T_{\perp {\rm e}} = Tr\boldsymbol{T}_{\rm e}$, including the off-diagonal components responsible for nongyrotropic (crescent) features of the electron distribution function $f_{\rm e}$ and the temperature tensor $\boldsymbol{T}_{\rm e} \equiv \boldsymbol{P}_{\rm e}/(nk)$. The electric field given by Equation (4) becomes important in the region where ions decouple and electron physics dominate. Hence, we propose that the ratio of the thermal pressure term in Equation (4) to the sum of other terms including the ideal with Hall term $\boldsymbol{E}'$, Equation (2), and the electron (inertial) accelerating $\boldsymbol{E}_{\rm a}$ contributions, Equation (3), $r_{\rm e} \equiv |\boldsymbol{E}_{\rm p}|/|\boldsymbol{E}' + \boldsymbol{E}_{\rm a}|$, to be a signature indicating approaches to the EDR.

The *MMS* mission was launched in 2015 to investigate magnetic reconnection near the Earth's magnetopause and in

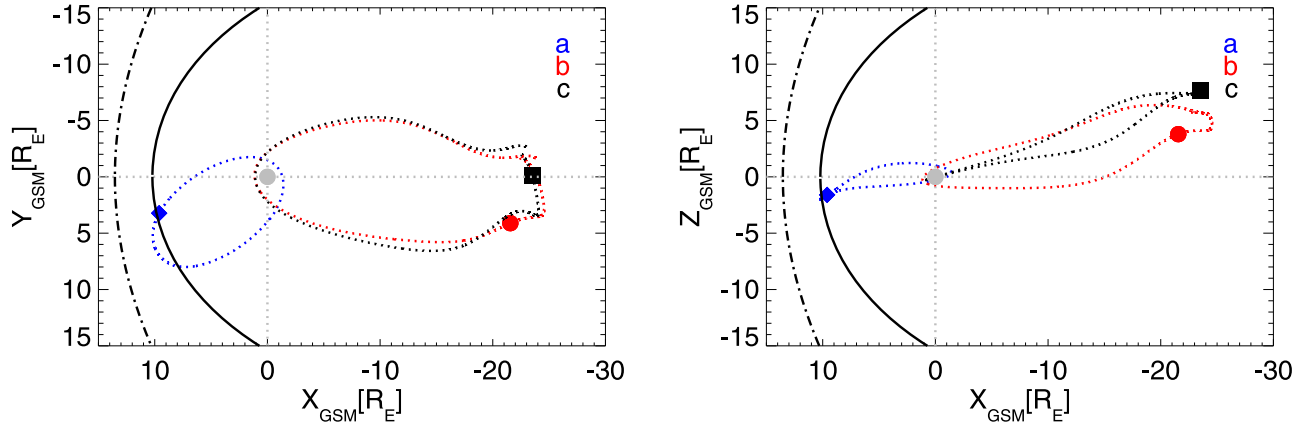

Figure 1. *MMS* spacecraft trajectories and positions inside the magnetosphere near crossing of the magnetopause (a) in 2016 November and the magnetotail (b) in 2017 July and 2018 July 24 (c), respectively.

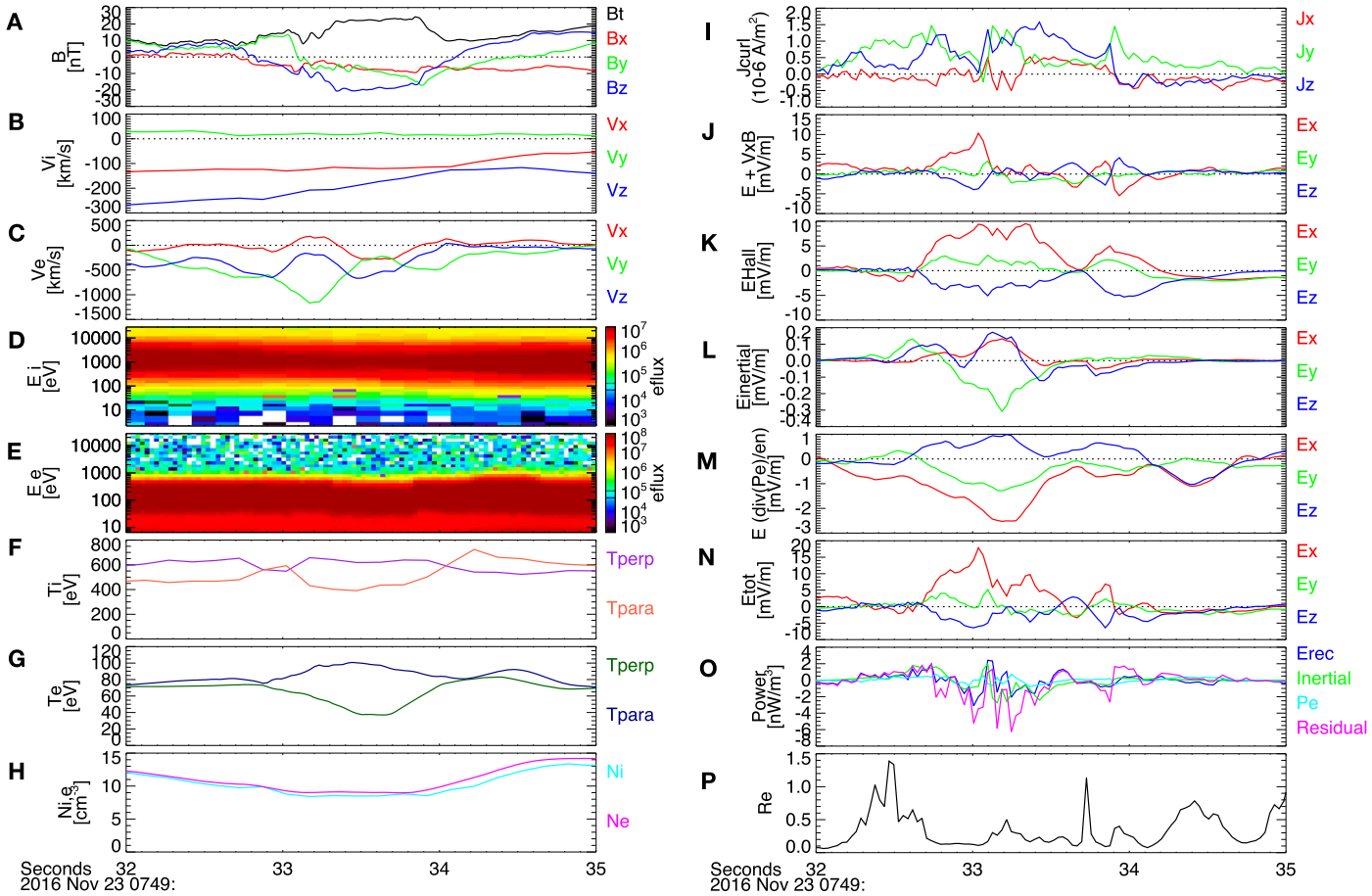

Figure 2. Data and various electric fields identified by *MMS* 2 spacecraft when crossing the magnetopause on 2016 November 23 centered around 07:49:33.5, case (a) in Table 1: (A) magnetic field $\boldsymbol{B}$ vector components, ion (B) and electron (C) velocity vectors, ion (D) and electron (E) energy spectra, and the ion (F) and electron (G) perpendicular $T_\perp$ and parallel $T_\parallel$ temperatures with density n_i and n_e (H); current $\boldsymbol{j}$ (I) with various obtained electric field components contributions to the generalized Ohm's law: ideal $\boldsymbol{E} + \boldsymbol{V} \times \boldsymbol{B}$ (J), Hall $\boldsymbol{E}_H$ (K), inertial acceleration $\boldsymbol{E}_a$ (L), electron pressure $\boldsymbol{E}_p$ (M), and residual (anomalous) $\eta\boldsymbol{j}$ (N) terms, respectively. The electromagnetic energy density (power $W = \boldsymbol{j} \cdot \boldsymbol{E}$) converted to plasma energy from various terms of $\boldsymbol{E}$ (O) with the reconnection parameter r_e in the last panel (P).

the magnetotail (Burch et al. 2016a). This Letter compares reconnection in different regions of the magnetosphere. Figure 1 shows the *MMS* trajectories for cases (a)–(c) that will be presented in Figures 2–4, respectively, in the Geocentric Solar Magnetospheric (GSM) coordinates (x toward the Sun, y toward dusk, with the dipole axis in the x, z plane), similar to the (L, M, N) coordinates used in by Torbert et al. (2016, 2018). Table 1 lists the respective time intervals with chosen characteristics (calculated when B_x changes sign): $\boldsymbol{j}$, $\boldsymbol{E}_H$, including the parameter, $r_e \equiv |\boldsymbol{E}_p|/|\boldsymbol{E}' + \boldsymbol{E}_a|$, postulated to be signature indicating approaches to the EDR, the residual (anomalous) dissipation field $\boldsymbol{E}_{tot} = \eta\boldsymbol{j}$, and the energy density (power W) that should be dissipated by this (total) anomalous term in the generalized Ohm's law, Equation (1).

For the magnetic field $\boldsymbol{B}$, we use BURST-type observations from the FluxGate Magnetometers (FGM; Russell et al. 2016)

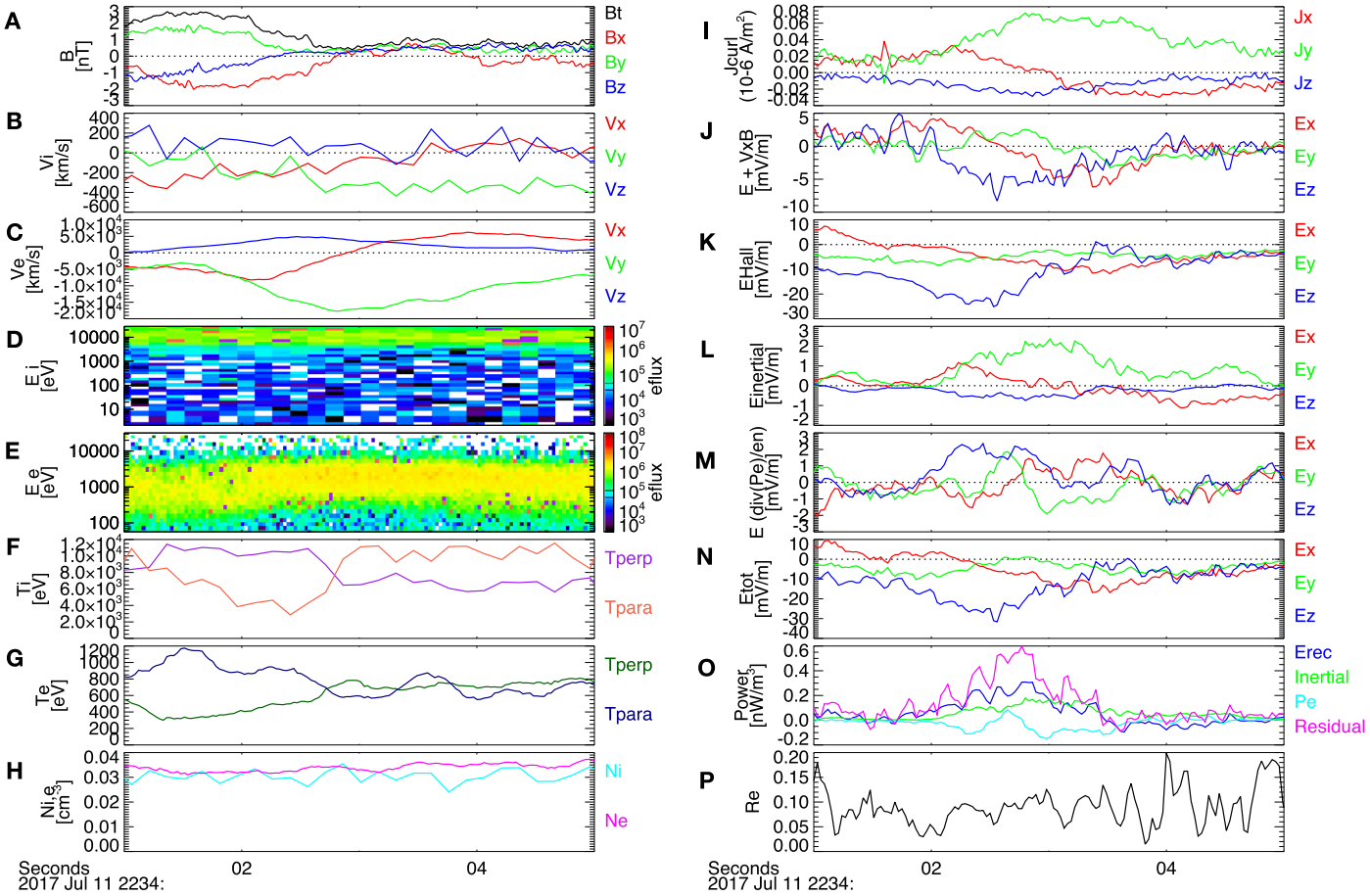

Figure 3. Data and various electric fields identified by *MMS* 3 spacecraft when crossing the magnetotail on 2017 July 11 centered around 22:34:03, case (b) in Table 1.

with the highest cadence of 7.8 ms (survey data have substantially lower time resolutions of 0.0625–0.125 s). For the ion and electron plasma velocities, $\boldsymbol{V_i}$ and $\boldsymbol{V_e}$, we use observations measured by the Dual Ions and Electron Spectrometer instruments (DIS and DES; Pollock et al. 2016), with somewhat lower time resolution. During BURST observations we have 150 ms sampling for ions and 30 ms for electrons, respectively (in FAST-type observations, the instruments provide moments each of 4.5 s). On 2018 June 7 *MMS* 4 suffered an anomaly, and from 2018 July 15 two quadrants of the electron spectrometer are turned off. Using the highest-resolution data available for one of many magnetopause 4 s intervals in 2016 that have been analyzed by Webster et al. (2018), specified as case (a) in Table 1, we have 513 measurement points for the magnetic field and 133 (27) points for the electron (ion) velocity. However, it appears that reconnection in the magnetotail is much more difficult to identify. Inside the magnetosphere, when approaching the EDR in the magnetotail on 2017 July 17, the 4 s interval has only been reported by Torbert et al. (2018), and we analyze this case (b), as listed in Table 1. We also consider another interval lasting 8 s during a magnetotail crossing on 2018 July 24 consisting of 1026 points for the magnetic field $\boldsymbol{B}$ and 267 (53) points for the ion and electron $\boldsymbol{V}_{\rm i,e}$ velocity, case (c) in Table 1.

The left panels ((A)–(H)) of Figures 2–4 display the data used for the analysis. Because all probes observed similar structures, we display the data for only one selected *MMS* spacecraft for each event. The magnetic field vector components including its magnitude are presented in panel (A), with all components of the ion (B) and electron (C) velocity vectors, the ion (D) and electron (E) energy omnidirectional spectrograms, the ion (F) and electron (G) perpendicular $T_\perp$ and parallel $T_\parallel$ temperatures, and the ion and electron density $n_{\rm i}$ and $n_{\rm e}$ are shown in the bottom panel (H).

We see that the components of the magnetic field $B_{\rm x}$ and $B_{\rm z}$ change sign at 7:49:33, 22:34:03, and 17:47:10, respectively, and that the ion V_{ix} velocity usually changes sign nearly simultaneously, followed by distinct fast electron jets V_{ex}. When densities are low in the magnetotail (0.1–0.3 cm^{-3}) we reduce the noise caused by local photoelectrons from the spacecraft by including only particles with energies greater than 56 eV (165 eV) for electrons and 975 eV for ions (panels E) in the respective partial distribution functions for cases (b) and (c), see Supplementary Materials of Torbert et al. (2018). Because the highest resolutions available for the ion distributions are 5 times lower than that for electrons, we have also verified that the fluctuations in the electron speeds could be smoothed by using somewhat lower resolutions for electrons. A reversal in ion flow is still clearly seen in all panels (B) but substantial variations in electron speeds are present in panel (C) only in case (c), smoothed by the same running averages of 0.3 s (twice the resolutions for ions, 0.15 s), and to be consistent with quasi-neutrality achieved in panel (H). Contrary to case (b) of 2017 July 11, when MMS crossed the EDR region (Torbert et al. 2018), in case (c) representing the current sheet crossings in 2018 we see large chaotic fluctuations in the electron velocities. In fact, this may exhibit some turbulent processes responsible for reconnection when approaching or

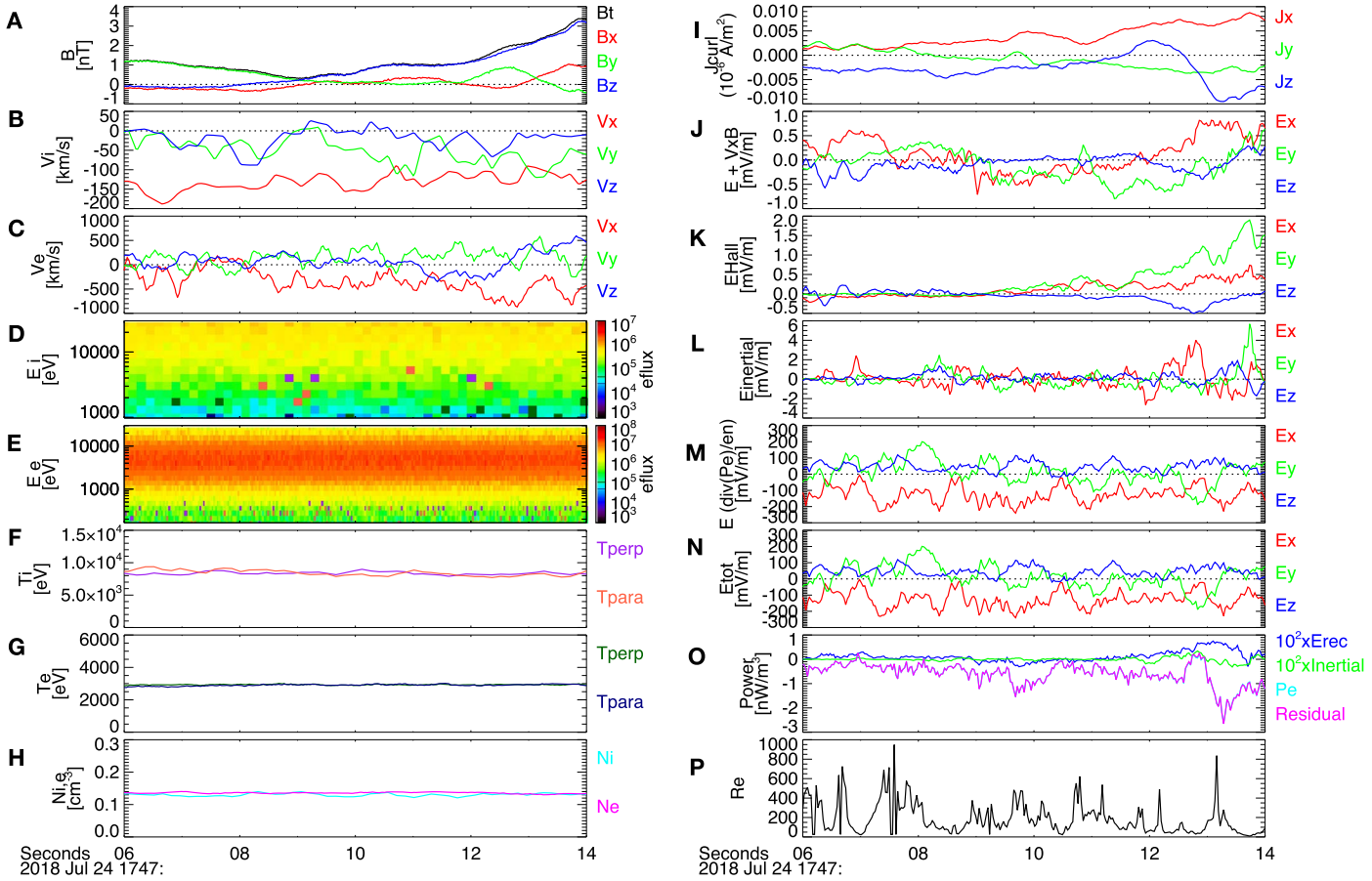

Figure 4. Data and electric fields identified by *MMS* 2 spacecraft when crossing the magnetotail on 2018 July 24 centered around 17:47:10, case (c) in Table 1.

passing by the *X*-line. Besides the flow reversal, some heating is observed here for both ions (up to energies of a few tens keV) and electrons (1–10 keV), but compared with the temperature asymmetry observed in the EDR of 2017 July 11, for the current sheet crossing on 2018 July 24 roughly isotropic ion (3–6 keV) and electron temperatures (2–3 keV), are seen in panels (D) and (E).

The main results for the reconnecting electric fields are shown in the right panels from (I) to (P) of Figures 2–4. First, the current $\boldsymbol{j}$ obtained from the curl of the magnetic field $\boldsymbol{B}$ is displayed in panel (I). The relatively large components during the crossing of the current sheet are seen especially at the magnetopause, case (a). Next, besides the ideal field $\boldsymbol{E} + \boldsymbol{V} \times \boldsymbol{B}$ (1–10 mV m^{-1}) seen in the frame of the plasma moving with the bulk speed $\boldsymbol{V}$ (panel J), we display nonideal electric fields resulting from the following terms: the Hall $\boldsymbol{E}_{\rm H}$ (panel K), inertial acceleration $\boldsymbol{E}_{\rm a}$ (L), and electron pressure $\boldsymbol{E}_{\rm p}$ (M) electric fields, respectively. The Hall electric fields of Equation (2) have been calculated using two methods, from Ampere's law (curl of the magnetic field) and from plasma ion and electron data, to check the consistency of the calculations of moments of electron distribution functions (only the curlometer current is shown in panel (I)). The divergence of the ion and electron velocity tensors in Equation (3) and the electron pressure tensor of Equation (4) have been calculated using the probability distribution functions with the tools developed for analysis of multispacecraft data employing a linear interpolation within the tetrahedral configuration of four spacecraft (in case (c), only MMS 1, 2, and 3 are taken; Chanteur 2000, chapter 14).

It is interesting to compare the electric fields contributing to the generalized Ohm's law as displayed in panels (J)–(M). We see that the electric field resulting from the Hall current (1–10 mV m^{-1}) is the same order as the ideal field, and as expected the Hall term still plays an important role for fast reconnection, especially in the IDR. The contribution from the inertial term is rather small at the magnetopause, case (a) (fraction of mV m^{-1}), and moderate in the magnetotail (1–2 mV m^{-1}) in cases (b) and (c). In particular, we have recovered the current and magnetic field at the magnetopause, case (a), but we have noticed that $\boldsymbol{E}_{\rm H} = -\boldsymbol{j} \times \boldsymbol{B}/(en)$ can provide values up to 10 mV m^{-1}, i.e., larger than the inertial contribution, contrary to Webster et al. (2018; owing to the corrected multiplication error in their Figure 8).

On the other hand, as compared with the rather small reconnection electric fields of 1–2 mV m^{-1} at the magnetopause, case (a), and in the EDR in 2017, case (b), we see a very large electric field up to 200 mV m^{-1} resulting from the divergence of the electron pressure gradient in the neutral sheet crossing in 2018, case (c). Please note that Hall physics is in principle dissipationless, $W_{\rm H} = \boldsymbol{j} \cdot \boldsymbol{E}_{\rm H} = -\boldsymbol{j} \cdot (\boldsymbol{j} \times \boldsymbol{B})/(en) = 0$. Hence, the secondary Hall electric field can only accelerate a small group of electrons. However, the divergence of the electron pressure term is clearly dissipative, because it introduces electron velocities, Equation (4). This shows that, when electrons decouple from ions, electron kinetic physics should play a major role in the neutral sheet reconnection site.

Table 1
List of Selected *MMS* Spacecraft (s-c) Interval Samples in the Magnetopause (a) and the Magnetotail (b, c) (hh.min:ss)

Case	S-c	Time (y.m.d)	Begin	End	$\boldsymbol{j}$ (μA/m2)	$\boldsymbol{E}_{\rm H}$ (mV m^{-1})	$\eta\boldsymbol{j}$	W (nW/m3)	$r_{\rm e}$
(a)	2	2016 Nov 23	07.49:32	07.49:35	0.454	7.89	15.45	−3.07	0.10
(b)	3	2017 Jul 11	22.34:01	22.34:05	0.0644	11.86	17.37	0.247	0.08
(c)	2	2018 Jul 24	17.47:06	17.47:14	0.0056	0.20	207	−0.994	207

The sum of these contributions $\boldsymbol{E}_{\rm tot}$, Equation (1), is displayed in panel (N), which is attributed to anomalous (residual) $\eta\boldsymbol{j}$ electric field. The electromagnetic energy density (power $W = \boldsymbol{j}\cdot\boldsymbol{E}$) converted to plasma energy from these terms (besides zero contribution from the Hall current) is shown in the bottom panel (O). Finally, the parameter $r_{\rm e} \equiv |\boldsymbol{E}_{\rm p}|/|\boldsymbol{E}' + \boldsymbol{E}_{\rm a}|$ in panel (P) is our proposed signature indicating proximity to the electron dissipation (EDR) reconnection site. In fact, as seen in the last panel (P) this value is small at the magnetopause (up to 1.5) but becomes large near the neutral sheet (10–15), and substantially increases (two order of magnitudes) when approaching the *X*-line where reconnection takes place.

In conclusion, following various observations of reconnection at the magnetopause and the first crossing of the EDR in the magnetotail by *MMS* on 2017 July 11 reported by Torbert et al. (2018), we have studied a new *MMS* event on the nightside magnetosphere at the current sheet on 2018 July 24. The observed magnetic field reversal on the current sheet approach is followed by an ion flow reversal, but with large fluctuations in the electron velocity. Compared with the temperature asymmetry observed in the EDR of 2017 July, this approach to the neutral sheet charged particle exhibits some heating up to energies of a few tens keV for ions and 1–10 keV for electrons, but with rather isotropic ion (3–6 keV) and electron temperatures (2–3 keV).

In addition to ideal electric fields, our cases exhibit a large electric field comparable in magnitude (1–10 mV m^{-1}) to those associated with the Hall current, which together with the rather moderate inertial accelerating fields (1–2 mV m^{-1}), are responsible for fast reconnection in the IDR. However, during the approaches to the EDR, as indicated by our newly devised reconnection parameter, the electric fields arising from the divergence of the full electron pressure tensor provide the main contribution (as large as 200 mV m^{-1}) to the generalized Ohm's law. We can hence expect that when ions decouple electron kinetic physics should provide the mechanisms responsible for reconnection processes. The *MMS* mission may also be useful for better understanding the physical mechanism governing reconnection processes in various laboratory and astrophysical plasmas.

We are grateful for the dedicated efforts of the entire *MMS* mission team, including development, science operations, and the Science Data Center at the University of Colorado. We especially benefited from the efforts of C. J. Pollock, and C. T. Russell and the magnetometer team for providing the magnetic field data, available online from http://cdaweb.gsfc.nasa.gov. We acknowledge T. E. Moore, a Project Scientist, and M. L. Adrian, Deputy Project Scientist, for discussions on the field and plasma instruments.

ORCID iDs

W. M. Macek https://orcid.org/0000-0002-8190-4620
M. V. D. Silveira https://orcid.org/0000-0002-9614-3975
D. G. Sibeck https://orcid.org/0000-0003-3240-7510
B. L. Giles https://orcid.org/0000-0001-8054-825X
J. L. Burch https://orcid.org/0000-0003-0452-8403

References

Baumjohann, W., & Treumann, R. A. 1996, Basic Space Plasma Physics (London: Imperial College Press)
Biskamp, D. 2000, Magnetic Reconnection in Plasmas, Vol. 3 (Cambridge: Cambridge Univ. Press)
Bruno, R., & Carbone, V. 2016, Turbulence in the Solar Wind, Vol. 928 (Berlin: Springer International Publishing)
Burch, J. L., Moore, T. E., Torbert, R. B., & Giles, B. L. 2016a, SSRv, 199, 5
Burch, J. L., Torbert, R. B., Phan, T. D., et al. 2016b, Sci, 352, 2939
Burlaga, L. F. 1995, Interplanetary Magnetohydrodynamics (New York: Oxford Univ. Press)
Chanteur, G. 2000, in Analysis Methods for Multi-Spacecraft Data, ed. G. Paschmann & P. W. Daly (Bern: ISSI Scientific Report), 349
Daughton, W., Nakamura, T. K. M., Karimabadi, H., Roytershteyn, V., & Loring, B. 2014, PhPl, 21, 052307
Figura, P., & Macek, W. M. 2013, AnPhy, 333, 127
Gurnett, D. A., & Bhattacharjee, A. 2005, Introduction to Plasma Physics (Cambridge: Cambridge Univ. Press)
Krall, N. A., & Trivelpiece, A. W. 1973, Principles of Plasma Physics (New York: McGraw-Hill)
Landau, L. D., Lifshitz, E. M., & Pitaevskii, L. P. 1984, Electrodynamics of Continuous Media, Vol. 8 (Oxford: Pergamon)
Lazarian, A., Eyink, G., Vishniac, E., & Kowal, G. 2015, RSPTA, 373, 20140144
Liu, H., Zong, Q.-G., Zhang, H., et al. 2019, NatCo, 10, 1040
Macek, W., & Grzedzielski, S. 1985, in Twenty Years of Plasma Physics, ed. B. McNamara (Singapore: World Scientific), 320
Macek, W. M., Krasińska, A., Silveira, M. V. D., et al. 2018, ApJL, 864, L29
Macek, W. M., Silveira, M. V. D., Sibeck, D. G., Giles, B. L., & Burch, J. L. 2019, GeoRL, 46, 10295
Nakamura, T. K. M., Genestreti, K. J., Liu, Y.-H., et al. 2018, JGR, 123, 9150
Øieroset, M., Phan, T. D., Haggerty, C., et al. 2016, GeoRL, 43, 5536
Pollock, C., Moore, T., Jacques, A., et al. 2016, SSRv, 199, 331
Rossi, B., & Olbert, S. 1970, Introduction to the Physics of Space (New York: McGraw-Hill)
Russell, C. T., Anderson, B. J., Baumjohann, W., et al. 2016, SSRv, 199, 189
Spitzer, L. 1956, Physics of Fully Ionized Gases (New York: Interscience)
Strumik, M., Czechowski, A., Grzedzielski, S., Macek, W. M., & Ratkiewicz, R. 2013, ApJL, 773, L23
Strumik, M., Grzedzielski, S., Czechowski, A., Macek, W. M., & Ratkiewicz, R. 2014, ApJL, 782, L7
Torbert, R. B., Burch, J. L., Giles, B. L., et al. 2016, GeoRL, 43, 5918
Torbert, R. B., Burch, J. L., Phan, T. D., et al. 2018, Sci, 362, 1391
Treumann, R. A. 2009, A&ARv, 17, 409
Treumann, R. A., & Baumjohann, W. 2013, FrP, 1, 31
Vasyliunas, V. M. 1975, RvGSP, 13, 303
Wang, R., Lu, Q., Nakamura, R., et al. 2018, GeoRL, 45, 4542
Webster, J. M., Burch, J. L., Reiff, P. H., et al. 2018, JGR, 123, 4858
Yamada, M., Yoo, J., & Myers, C. E. 2016, PhPl, 23, 055402
Yordanova, E., Vörös, Z., Varsani, A., et al. 2016, GeoRL, 43, 5969